https://doi.org/10.3311/PPch.41153

Periodica Polytechnica Chemical Engineering, 69(4), pp. 545–558, 2025

Application of Response Surface Methodology for the Adsorptive Removal of Chromium Using Modified Cellulose

Selvakumar Ponnusamy[1*], Saravanan Rajayyan[2], Vivek Kumar Chandrakumar[3], Jagadeeswari Rangaraman[2], Karthikeyan Rajagopalan[4]

[1] Department of Humanities and Science, Gokaraju Rangaraju Institute of Engineering and Technology, Hyderabad 500090, Telangana, India
[2] Department of Chemistry, KPR Institute of Engineering and Technology, Coimbatore 641407, Tamil Nadu, India
[3] Department of Civil Engineering, Gokaraju Rangaraju Institute of Engineering and Technology, Hyderabad 500090, Telangana, India
[4] Department of Mechanical Engineering, Gokaraju Rangaraju Institute of Engineering and Technology, Hyderabad 500090, Telangana, India
* Corresponding author, e-mail: selvakumarpr@mail.com

Received: 29 May 2025, Accepted: 12 September 2025, Published online: 28 October 2025

Abstract

In this study, a Modified Cellulose Polymer (MCP) was synthesized through selective oxidation in a cellulose polymer utilizing sodium periodate ($NaIO_4$), which introduces benzothiazole as a functional attachment without disrupting the cellulose backbone. Response surface methodology was employed for the adsorption of chromium on MCP, and the process parameters were optimized. Three critical process parameters, particle size (398-498 nm), pH (5-7), and adsorbent dose (20-30 mg/L), were optimized to obtain the optimal response of chromium adsorption using the statistical Box–Behnken design. The experimental data obtained were analyzed using analysis of variance (ANOVA) and fitted to a second-order polynomial equation using multiple regression analysis. Numerical optimization, utilizing the desirability function, was employed to determine the optimal conditions for maximum chromium ion removal. A two-level fractional factorial model and the Box-Behnken matrix were employed to optimize the batch adsorption parameters for the adsorption of chromium from aqueous solutions by modified cellulose. Under the optimized conditions of pH 6.04 ± 0.05, particle size 485.49 ± 2 nm, and adsorbent dose of 24.14 ± 0.5 mg/L, MCP demonstrated the maximum chromium adsorption capacity with a desirability score of 0.805. The batch adsorption experiments confirmed the efficacy of MCP in removing chromium from aqueous solutions, as evidenced by the close alignment between the predicted adsorption capacity (134.53 ± 1.8 mg/g) and the experimental result (132.52 ± 2,1 mg/g). These findings highlight the potential of MCP as an effective and environmentally friendly adsorbent for industrial water-treatment applications.

Keywords

response surface methodology, selective oxidation, adsorption, modified cellulose polymer

1 Introduction

Chromium-containing chemicals are extensively utilized in numerous industries, including leather tanning, chrome ore mining, metal finishing, pigment manufacturing, and wood preservation [1]. The acceleration of industrialization over the past few decades has resulted in an increase in chromium levels in aquatic and terrestrial ecosystems [2]. Regulations exist regarding the permissible threshold of chromium content in water and soil. Many countries have established 50 μg/L as the maximum permissible limit for total chromium in drinking water [3]. Contamination of water and soil can indirectly affect human health; consequently, the remediation of chromium has consistently been a focal point in heavy metal pollution treatment.

Conventional methods for treating heavy metal contamination include chemical precipitation, ion exchange, membrane separation, reverse osmosis, evaporation, electrochemical treatment, and adsorption [4]. Among these, the adsorption method has garnered significant attention in recent years because of its operational simplicity, recoverability of heavy metal ions, recyclability of adsorbents, and efficacy, particularly in the treatment of wastewater with low concentrations of heavy metals (<50 mg/L). Polymers employed as adsorbents can be classified into

Cite this article as: Ponnusamy, S., Rajayyan, S., Chandrakumar, V. K., Rangaraman, J., Rajagopalan, K. "Application of Response Surface Methodology for the Adsorptive Removal of Chromium Using Modified Cellulose", Periodica Polytechnica Chemical Engineering, 69(4), pp. 545–558, 2025. https://doi.org/10.3311/PPch.41153

synthetic polymers, hybrid polymers, natural polymers, and modified natural polymers [5]. Natural polymers have received considerable attention owing to their cost-effectiveness and availability. Notably, modified natural polymers combine the advantages of both synthetic and natural polymers and have demonstrated enhanced adsorption capacities. Cellulose, lignin, tannin, chitin, chitosan, and polypeptides are inexpensive and abundant natural polymers that are renewable, biodegradable, and non-toxic. The large number of hydroxyl groups present in cellulose limits its ability to bind to the metal. However, these hydroxyl groups are advantageous for grafting functional groups or molecules onto the cellulose structure, thereby improving adsorption capacity [6]. Although abundant hydroxyl groups are present in cellulose, its high crystallinity and strong hydrogen bonds among its chains restrict the accessibility of the surface hydroxyl groups and limit their practical applications [7]. Consequently, numerous studies have focused on improving the adsorption capacity of cellulose-based materials through these hydroxyl groups to initiate free radical reactions, esterification, halogenation, oxidation, and etherification [8]. Arredondo et al. developed a novel, environmentally sustainable, cellulose-based superabsorbent polymer called Cellulo-SAP, which can be readily prepared by radical-free synthesis employing modified cellulose [9]. Its adsorption, thermal/pH stability, reusability, and biodegradability were evaluated, and this innovative polymer demonstrated excellent pH and temperature stability, as well as versatility as a water reservoir. Saravanan et al. contributed to the synthesis of modified cellulose bearing pendant complexating compounds such as benzalaniline [10], hydroxyl [11], pyridine [12], carboxylic acid [13], and heterocyclic moieties [14], which function as chelating sites for the effective removal of Cu(II) and Pb(II) heavy metals from aqueous solutions. Response surface methodology (RSM) is essential for the successful implementation and commercialization of adsorption processes because of its capacity to optimize parameters, reduce experimental costs, and predict adsorption performance under varying conditions [15]. It provides a comprehensive understanding of the relationships between different variables, enabling efficient process design, scaling up, and ensuring consistent, and cost-effective performance, which are critical for industrial adoption and widespread application. Recent studies have illustrated its effectiveness in optimizing the removal of heavy metals and dyes [16]. Additional research emphasizes its capability to scale up adsorption systems and verify model predictions under various environmental conditions [17–19]. More recently, RSM has been effectively integrated with hybrid modelling techniques to improve the process accuracy [20–23]. Collectively, these studies highlight the dependability and predictive capability of RSM for optimizing the adsorption processes for wastewater treatment applications. Therefore, this study focused on the application of pendant group, Modified Cellulose-based Polymers (MCPs) for unexplored chromium removal from aqueous solutions and the optimization of the adsorption process in consideration of the commercialization of this polymer as a potential adsorbent.

2 Experimental

2.1 Materials and physical measurements

Cellulose (Loba), dimethyl formamide (Loba), sodium metaperiodate (Sigma-Aldrich), 2-aminobenzothiazole (Sigma-Aldrich) were used as received. The metal salt of $CrCl_3 \cdot 6H_2O$ (Loba) was used to prepare the stock Cr(III) solutions. All other chemicals and solvents used were of analytical grade or purified according to standard procedures [24]. Fourier transform infrared (FTIR, PerkinElmer, USA) and solid-state carbon-13 nuclear magnetic resonance (13C-NMR) spectra at 100.62 MHz on a Bruker AMX-200 spectrometer (Bruker, Germany) were used to determine the chelating groups that are responsible for the complexation of the modified cellulose polymer (MCP) adsorbent with the metal ions. The surface morphologies of the adsorbent and the metal-chelated adsorbent were analyzed using a Leo Gemini 1530 microscope (Carl Zeiss, Germany). In addition, the surface roughness was analyzed using the free program, Gwyddion. Using Gwyddion 2.58, the SEM images of the MCP were transformed into three-dimensional images.

2.2 Selective oxidation of cellulose

The modified cellulose polymer was synthesized according to a previously reported procedure [11, 13]. Periodate oxidation of cellulose was performed using $NaIO_4$ as the oxidizing agent, cleaving the C2–C3 bond of the glucosidic ring to convert 2,3-dihydroxyl groups into 2,3-dialdehyde (DAC) groups via the Malaprade reaction [25]. $NaIO_4$ was prepared in deionized water, and the cellulose powder was treated in the dark at ambient temperature with continuous stirring for 4 h, achieving 30 carbonyl groups per 100 glucose units. DAC reacts with amine compounds to form Schiff base derivatives. In this study, carboxymethyl cellulosebased Schiff base was synthesized by condensing

dialdehyde cellulose (DAC) with aminobenzothiazole in dimethylformamide at 343 K for 5 h. The precipitate was then filtered, washed, and dried. The MCP synthesis scheme with chelating groups is shown in Scheme 1.

2.3 Adsorption of chromium

In the present study, batch adsorption experiments were conducted to investigate the adsorption isotherms and kinetic mechanism for the removal of Cr(III) ions under optimum conditions. A calculated amount of adsorbent was added to 100 mL of Cr(III) solution with a concentration ranging from 100–500 mg/L shaken on a horizontal bench shaker at 200 rpm (Orbitek-Teqip-ACT/EQ/454, Tamil Nadu, India). After equilibrium, the supernatant was analyzed. Various operating parameters such as pH, contact time, adsorbent dose, initial metal ion concentration, temperature (303 K) and regeneration performance were investigated to determine the most favourable conditions for the removal of Cr(III) ions by MCP. The optimization ranges (particle size: 398–498 nm, pH: 5–7, adsorbent dose: 20–30 mg/L) were chosen based on preliminary trials and literature to ensure MCP stability and practical feasibility [13]. The percentage removal (% E) and amount of metal ions adsorbed onto MCP at equilibrium (q, mg/g) were calculated using the following equations [26];

$$\%E = \left(1 - \frac{C_e}{C_0}\right) \times 100 \tag{1}$$

$$q = \frac{(C_0 - C_e)V}{m}, \tag{2}$$

where C_0 and C_e are the initial and equilibrium final concentrations (mg/L) of the metal ion solutions, respectively,

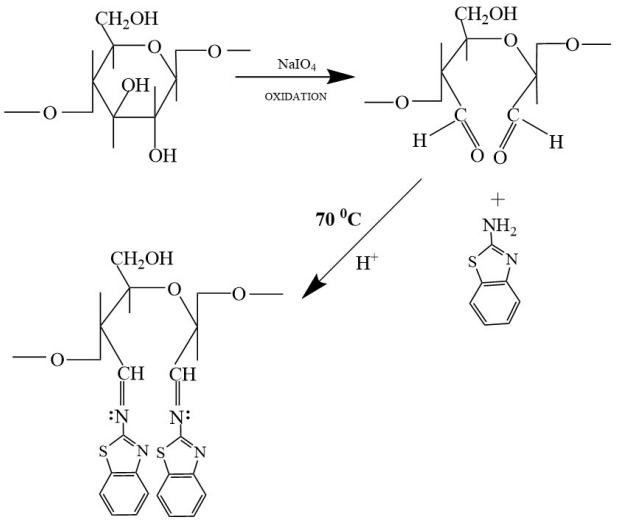

Scheme 1 The MCP synthesis

V is the volume of the solution (L), and m is the mass of the adsorbent MCP (g).

2.4 Box–Behnken design

The RSM and Box–Behnken statistical experimental design were used to examine how the three independent factors affected the response function. The particle size (X_1), adsorbent dosage (X_2), and pH (X_3) were the independent factors. As seen in Table 1, the low, centre and high levels of each variable are designated by the numbers 1, 0, and +1, respectively. Initial experimental findings were used to determine the experimental levels for each variable. The percentage of chromium adsorption was used as the response variable. The variables were coded according to the following equation [27]:

$$X_i = \frac{\left(X_i - X_0\right)}{\Delta X_i} \tag{3}$$

The dimensionless value of an independent variable is denoted by X_i, the real value X_i, the real value at the centre point by X_0, and the step change in the real value of the variable ΔX_i representing a variation of one unit for the dimensionless value of variable 'i' is denoted by X_i. The formula for the number of tests (N) required to generate the Box-Behnken matrix is $N = 2 \times k \times (k–1) + r$, where k is the factor number and r is the replicate number of the central point.

The present investigation used a total of 17 examinations to assess how the three primary independent characteristics affected the chromium adsorption efficiency. Table 2 lists the experimental setup matrix in its actual form.

The process performance was assessed by examining the response (y), which is dependent on the input components X_1, X_2,…X_k. The following formula describes the relationship between the response and the input process variables.

$$y = f\left(X_1, X_2, X_3, ..., X_k\right) + \varepsilon, \tag{4}$$

where f is the real response function, whose format is unknown and e is the residual factor associated with the experiments. The surface represented by $f(X_i, X_j)$ is known as the response surface.

Table 1 Box–Behnken design factors and independent variables

Variables (Unit)	Factors	Levels		
		–1	0	1
Particle size (nm)	A	398	448	498
Dosage (mg/L)	B	20	25	30
pH	C	5	6	7

Table 2 Experimental design matrix (Box–Behnken) and experimental responses

Run	Particle size nm	Dosage mg/L	pH	Removal mg/g
1	448	20	7	98.7
2	498	30	6	87.21
3	448	25	6	153.5
4	448	25	6	127.57
5	448	20	5	107.53
6	448	30	7	95.52
7	398	25	7	121.42
8	498	25	5	97.62
9	448	30	5	87.6
10	498	25	7	104.63
11	498	20	6	109.78
12	448	25	6	153.4
13	448	25	6	153.1
14	398	25	5	148.56
15	398	20	6	137.5
16	398	30	6	137.42
17	448	25	6	143.7

The response can be represented graphically, either in three-dimensional space or as contour plots that help visualize the shape of the response surface. For RSM, the most commonly used second-order polynomial equation developed to fit the experimental data and determine the relevant model terms can be written as [28]:

$$y = \beta_0 + \sum \beta_0 X_i + \sum \beta_{ii} X_i^2 + \sum \beta_{ij} X_i X_j , \quad (5)$$

where β_0 is the constant coefficient, β_{ii} is the slope or linear effect of input factor X_i, β_{ij} is the linear by a linear interaction effect between input factor X_i and, b_{ii} is the quadratic effect of input factor X_i.

2.5 Desirability

The optimal performance levels for multiple responses can be determined by simultaneously determining the optimal settings for the input variables by using the desirability function approach. Two parts make up the desirability procedure: (1) determining the values of the independent factors that concurrently yield the most acceptable expected responses on the dependent variables, and (2) optimizing the overall desirability of the controllable elements [29]. In 1980, Derringer and Suich created an additional version [30]. The general approach is to first convert each response (y_i) into an individual desirability function (d_i) which varies over the range,

$$0 \le d_i \le 1 , \quad (6)$$

where if response y_i is at its goal or target, then $d_i = 1$, and if the response is outside an acceptable region, $d_i = 0$. The design variables were then chosen to maximize overall desirability:

$$D = \left(d_1 \times d_2 \times d_3 ... \times d_n\right)\frac{1}{n}, \quad (7)$$

where n is the number of responses to measure.

Depending on whether a particular response y_i is to be maximized, minimized or assigned a target value, the different desirability functions $d_i(y_i)$ used are those proposed by Derringer and Suich [29]. If a response is of the "target is the best" kind, then its individual desirability function is:

$$\begin{aligned} d_i &= \left(y_i - \frac{L_i}{T_i} - L_i\right) \times p \quad \text{if} \quad L_i \le y_i \le T_i \\ d_i &= \left(y_i - \frac{L_i}{T_i} - U_i\right) \times q \quad \text{if} \quad L_i \le y_i \le T_i \\ d_i &= 1 \quad \text{if} \quad y_i = T_i \\ d_i &= 0 \quad \text{if} \quad y_i = L_i \ \text{ or } \ y_i = L_i \end{aligned} , \quad (8)$$

where exponents p and q determine the importance of hitting the target value. If a response is maximized, the individual desirability is defined as shown in Eq. (9).

$$\begin{aligned} d_i &= 0 \quad \text{if} \quad y_i \le L_i \\ d_i &= \left(y_i - \frac{L_i}{T_i} - L_i\right) \times p \quad \text{if} \quad L_i \le y_i \le T_i \\ d_i &= 1 \quad \text{if} \quad y_i \ge L_i \end{aligned} \quad (9)$$

Finally, if a response is to be minimized, the individual desirability (d_i) is calculated according to Eq. (10).

$$\begin{aligned} d_i &= 1 \quad \text{if} \quad y_i \le T_i \\ d_i &= \left(y_i - \frac{U_i}{T_i} - U_i\right) \times q \quad \text{if} \quad T_i \le y_i \le U_i \\ d_i &= 0 \quad \text{if} \quad y_i \ge U_i \end{aligned} , \quad (10)$$

where L_i, U_i and T_i are the lower, upper and target values, respectively, which are desired for response y_i, with $L_i \le y_i \le U_i$.

2.6 Adsorption isotherm

Many equations can be used to analyze the experimental adsorption equilibrium data. In this study, the following three models were tested: Langmuir isotherm theory assumes monolayer coverage of the adsorbate over a homogenous adsorbent surface. The Langmuir equation [31] is formulated as:

$$q_c = \frac{Q_L b C_\in}{1 + b_T C_e} , \quad (11)$$

where Q_L is the maximum adsorption capacity of the adsorbent (mg/g), corresponding to the monolayer surface coverage, and b is the adsorption affinity constant or Langmuir constant (L/mg) and is a measure of the energy of adsorption.

The Freundlich isotherm is an empirical equation describing the adsorption on a heterogeneous surface [32]. The Freundlich isotherm is commonly presented in Eq. (12).

$$q_c = K_F C_e^{\frac{1}{n}}, \tag{12}$$

where K_F is the Freundlich constant related to the adsorption capacity (mg g^{-1})(mg $L^{-1})^{\frac{1}{n}}$ and n is the Freundlich exponent (dimensionless).

The Langmuir isotherm assumes that adsorption occurs at fixed, equivalent sites and that the heat of adsorption is constant. In contrast, the Temkin model assumes a linear decrease in adsorption energy, which makes it more suitable for describing non-ideal adsorption [33]. The model can be expressed in the form of an equilibrium adsorption isotherm:

$$q_e = \frac{RT}{b_T} \ln\left(K_T C_e\right), \tag{13}$$

where q_e is the amount of adsorbate at equilibrium, C_e is the equilibrium concentration of the adsorbate in the solution, and the terms R, T, K_T, and b_T is Temkin constant, have the same meanings as in Eq. (11).

2.7 Adsorption kinetics

To examine the mechanism controlling the adsorption processes, pseudo-first-order, pseudo-second-order, and intra-particle diffusion kinetic equations were used to test the experimental data. The pseudo-first-order equation of Lagergren is generally expressed as [33],

$$q_t = q_c\left(1 - \exp\left(-k_1 t\right)\right), \tag{14}$$

where k_1 1/min is the rate constant of the pseudo-first-order adsorption and t is the time. The pseudo-second-order equation based on the adsorption equilibrium capacity can be expressed as Eq. (15) [34]:

$$q_t = \frac{k_2 q_t^2 t}{1 + k_2^2 q_c t}, \tag{15}$$

where k_2 (g/(mg·min)) is the rate constant of pseudo-second-order adsorption. The intra-particle diffusion model [35] was applied to the kinetic data using the pore diffusion factor described by Eq. (16):

$$q_t = k_i \sqrt{t} + c, \tag{16}$$

where k_i is the intra-particle diffusion rate constant (mg/(g·min)$^{1/2}$) and c is the intercept (mg/g).

2.8 Model comparison

All the model parameters were evaluated by non-linear regression using MATLAB software [36], and the determination coefficient (R^2), sum of squares due to error SSE, residual root mean square error RMSE and chi-square test were also used to measure the goodness-of-fit. We used the second-order corrected Akaike Information Criterion (AIC_C) statistical approach to compare the models. The error functions employed were as follows:

(i) The sum of the squares of the errors:

$$SSE = \sum_{i=1}^{n}\left(q_{i(\exp)} - q_{i(\mathrm{mod})}\right)^2, \tag{17}$$

where $q_{i(exp)}$ is the adsorption capacity obtained from the experiment and $q_{i(mod)}$ is the adsorption capacity obtained from the kinetic model.

(i) The coefficient of determination:

$$R^2 = 1 - \frac{SSE}{SST}, \tag{18}$$

where SST is called the total sum of squares.

(i) The residual root means square error:

$$RMSE = \sqrt{\frac{1}{n-p}\sum_{i=1}^{n}\left(q_{i(\exp)} - q_{i(\mathrm{mod})}\right)^2} \tag{19}$$

(ii) Chi-square test:

$$\chi^2 = \sum_{j=1}^{\pi}\frac{\left(q_{i[eqp)} - q_{\mathfrak{i}(\mathrm{mod})}\right)^2}{q_{i(\mathrm{mod})}} \tag{20}$$

(iii) Corrected Akaike information criterion (AIC_C)

$$AIC_C = n\ln\frac{SSE}{n} + 2p + \frac{2p\left(p+1\right)}{n-p-1}, \tag{21}$$

where p is the number of parameters in the model, and n is the number of data points, AIC_C values can be compared using the evidence ratio E which is defined by:

$$E = \frac{1}{\exp\left(-0.5\Delta\right)}, \tag{22}$$

where Δ is the absolute value of the difference in AIC_C between the two models.

3 Result and discussion

3.1 Characterization

MCP is produced by the selective oxidation of cellulose and its condensation with aromatic amines. The chemical modification of cellulose was confirmed by FTIR and ^{13}C-NMR spectroscopy and the spectral data of the MCPs. Several peaks were observed in the spectrum of the native cellulose, indicating that it was composed of various functional groups. The intense main characteristic bands at 3348 cm^{-1} are attributed to –OH stretching, 2903 cm^{-1} (C–H), 1664 cm^{-1} (C–C ring), 1430 cm^{-1} (–CH_2), 1371 cm^{-1} (–CH bend) and 1058 cm^{-1} (C–O–C) which are in good agreement with previously reported values [11]. In MCP the –OH stretching frequency appeared at 3343 cm^{-1}, while the imine –CH stretching frequency appeared at 2895 cm^{-1}, 1536 cm^{-1} (C–N), 1448 cm^{-1} (–CH_2 bend), 888 cm^{-1} (C–S). The C–C ring stretching frequency was not observed in the modified cellulose owing to the cleavage of the pyranose ring.

A strong absorption peak at 1659 cm^{-1} is clear, which is due to the –N=CH– (azomethine) stretching frequency, supporting the configuration of the pendant benzothiazole groups in MCP shown in Fig. 1. The spectrum of native cellulose (Fig. 2) shows signals vibrating around δ = 62.2 to 102.4 ppm for carbons of the pyranose ring, and the carbon of –CH_2–OH signal visible at δ = 44.2 ppm are in concord with the reported values.

The modified cellulose pyranose ring carbons exhibit signals between δ = 68 to 107. Apart from the descriptive signals, aromatic ring carbons appeared at δ = 124 ppm, 134 ppm and 150 ppm. The imine (–CH=N–) carbon showed at δ = 174 ppm. The carbon of the –CH_2–OH

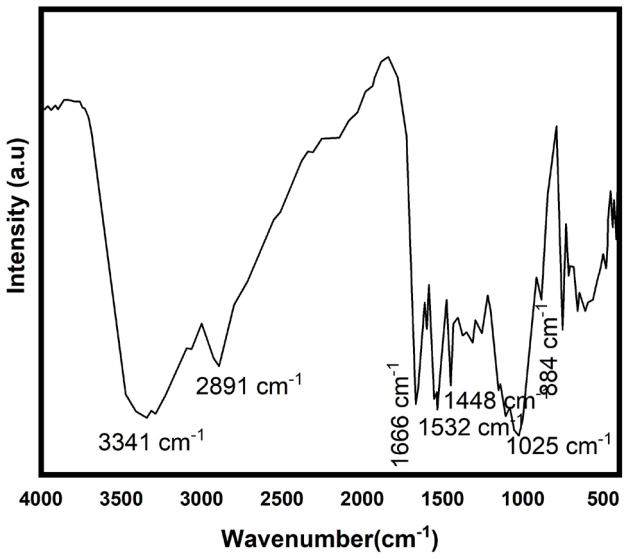

Fig. 1 FTIR spectrum of modified cellulose polymer

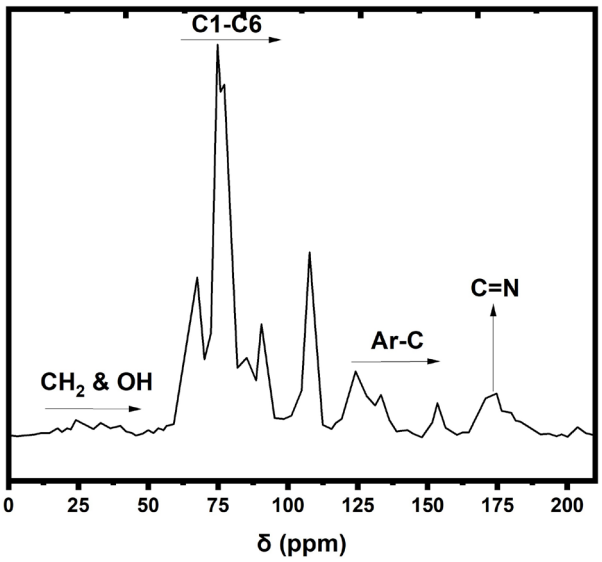

Fig. 2 NMR spectrum of modified cellulose polymer

group shifted to δ = 33 ppm. The pendant benzothiazole groups exhibit a broad signal at δ = 203 ppm. The assessment of the solid-state ^{13}C-NMR and FTIR spectra of the modified cellulose clearly showed that the formation of azomethine linkage and all the principal functional groups were present in the MCP backbone.

The MCP surface was more irregular, rough and had an open porous structure. The presence of pores in MCP suggests that metal ions are trapped and adsorbed on the surface. These cavities were sufficiently large to allow the metal ions to penetrate the surface and interact with the surface chelating groups. The surface morphology of the metal ion-adsorbed MCP showed layers of metal ions on the porous surface. The particle size was measured using a particle size analyzer and was found to be 448.3 ± 5.2 nm. The average particle size of the adsorbent provided a larger surface area for the removal of metals from aqueous media. By using Gwyddion mean roughness R_a was calculated and found as 355.4 ± 4.8 nm. Surface area and grain size were also calculated from a constructed 3D image of SEM (Fig. 3) and it was identified as 21.62 ± 0.35 × 10^6 and grain size as 480.1 ± 6.3 nm. The presence of more roughness and porosity facilitates the complexation of metals from aqueous solutions.

3.2 Box–Behnken Analysis

The analysis of variance (ANOVA) results used in the chromium adsorption investigation after the Box-Behnken responses are shown in Table 3. ANOVA was necessary to determine whether the model was adequate or significant. This breaks down the overall variance of the results into two sources: model and experimental errors [37]. This

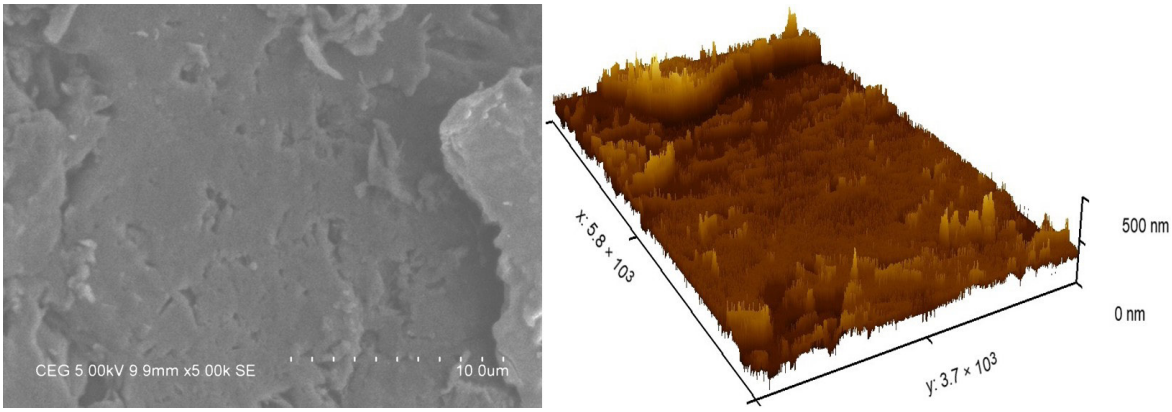

Fig. 3 SEM image and surface roughness of MCP

Table 3 ANOVA table for response surface quadratic model

Source	Sum of squares	df*	Mean square	*F*-value	*p*-value
Model	10270.05	9	1141.12	1000.46	< 0.0001
A-Particle size	3047.46	1	3047.46	2671.83	< 0.0001
B-Dosage	247.53	1	247.53	217.02	< 0.0001
C-pH	17.46	1	17.46	15.31	0.0058
AB	126.45	1	126.45	110.86	< 0.0001
AC	140.07	1	140.07	122.8	< 0.0001
BC	59.99	1	59.99	52.59	0.0002
A^2	107.03	1	107.03	93.84	< 0.0001
B^2	3316.81	1	3316.81	2907.98	< 0.0001
C^2	2709.36	1	2709.36	2375.4	< 0.0001
Residual	7.98	7	1.14		
Lack of fit	7.08	3	2.36	10.49	0.0229
Pure error	0.9005	4	0.2251		
Cor total**	10278.03	16			

* df = degrees of freedom; Between groups = groups − 1, Within groups = total − groups, Total = total − 1
** Corrected total = total variation around the overall mean

indicates that the model variation is important for the variation caused by residual error. For this comparison, The Fisher's F-test value was calculated as the ratio of the model mean square to the residual error [38]. The adequacy of the model's fit as demonstrated in Table 3, shows that the *F*-value achieved, 1000.46, is larger than the *F*-value (1.06 at 95% significance) derived from the standard distribution tables. Table 3 shows the p-values (Prob > *F*) employed to determine the importance of each term. With extremely low *p*-values ($p < 0.05$), the terms X_1, X_2, and X_3 are important, as can be seen in Table 3. The lack-of-fit test examines the pure error from the replicated design points with a residual error. Because the *p*-value is more than 0.05, the lack-of-fit *F*-value of 10.49 is not important. The non-significant lack-of-fit demonstrated the validity of the model for the current task. The resulted RSM model equation is as follows:

$$\begin{aligned}\text{Removal} = &-1108.35101 + 52.90302 \\ &\times \text{Particle size} + 192.95550 \times \text{pH} \\ &-0.022490 \times \text{Particle size} \\ &\times \text{Dosage} + 0.170750 \\ &\times \text{Particle size} \times \text{pH} + 0.837500 \\ &\times \text{Dosage} \times \text{pH} - 0.001511 \\ &\times \text{Dosage}^2 - 0.979930 \times \text{Dosage}^2 \\ &-24.41825 \times \text{pH}^2\end{aligned} \tag{23}$$

The particle size, dosage, and pH positively affected the chromium adsorption percentage, according to Eq. (23). An inverse relationship between the component and response is represented by a negative number, whereas a positive value denotes an influence that supports the optimization. The percentage effect of each factor was investigated using a Pareto analysis [39]. Based on the following relationship, the percentage effect (P_i) of each element on the response received was determined,

$$P_i = \left(\frac{\beta_i^2}{\sum_{i=1}^{14} \beta_i^2} \right) \times 100 \left(i \neq 0 \right), \tag{24}$$

where β_i denotes the regression coefficient of the individual process variables. Fig. 4 shows the Pareto graphic analysis. As can be seen in this figure, all three variables, particle size,

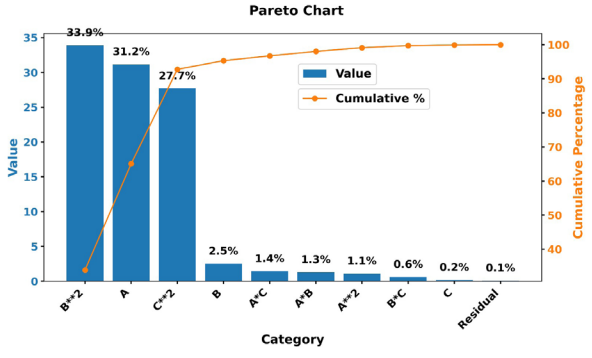

Fig. 4 Pareto chart with cumulative % contribution

dosage, and pH (β_2, 33.9%, β_1, 31.2% and β_3, 27.7%) produced the main effect on the percent chromium adsorption.

The R^2 of the model was 0.9992, indicating a good fit between the predicted values and experimental data points (Fig. 5). In addition, this implies that 99.92% of the variations in chromium adsorption percentage are explained by the independent variables, and this also means that the model does not explain only approximately 0.08% of the variation. The predicted R^2 value is a measure of how accurately the model predicts the response value. The adjusted R^2 and predicted R^2 should be within 0.20 of each other for reasonable agreement. If they are not, there may be a problem with either the data or model. In our case, the predicted R^2 value of 0.9888 is in reasonable agreement with the adjusted R^2 value of 0.9982. The adequate precision measures the signal-to-noise ratio and compares the range of the predicted values at the design points with the average prediction error. A ratio greater than 4 is desirable and indicates adequate model discrimination. In this study, the ratio was 77.90, indicating the reliability of the experimental data. The coefficient of variation (CV = 0.8643) and standard deviation (SD = 1.07) indicate the degree of precision. The low CV and SD values indicated the adequacy of the experiment.

The models had high R^2 values, significant F-values, insignificant lack-of-fit p-values and low standard deviations and coefficients of variance. These results indicate high precision in predicting the chromium removal efficiency of the MCP.

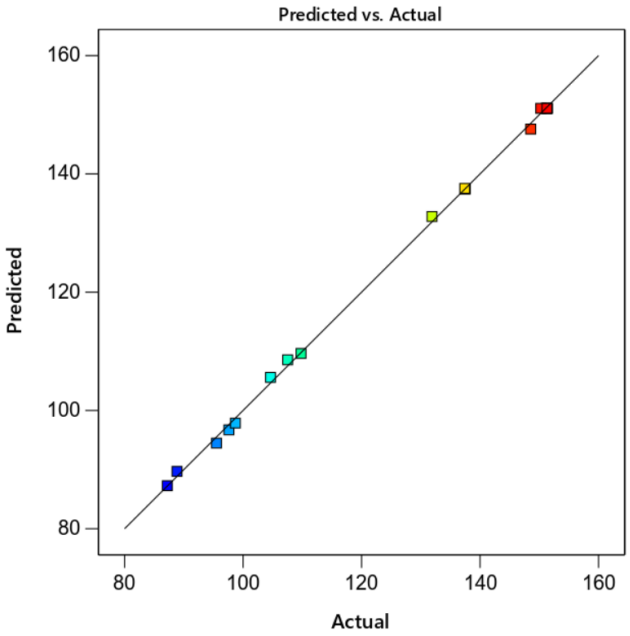

Fig. 5 Plot of the experimental and predicted responses

3.3 Optimization - desirability

Using numerical optimization, a desirable value for each input factor and response can be selected.

Therein, the possible input optimizations that can be selected include the range, maximum, minimum, target, none (for responses), and are set to establish an optimized output value for a given set of conditions. In this study, the input variables were given specific range values, and the response was designed to achieve a maximum. Under these conditions, the maximum chromium adsorption was 134.53 mg/g (Fig. 6) at an initial pH of 6.04 ± 0.05, particle size of 485.49 ± 2 nm, and adsorbent dose of 24.14 ± 0.5 mg/L. The confirmatory test results showed a chromium adsorption of 132.52 ± 2.1 mg/g under optimal conditions compared with the chromium adsorption of 134.53 ± 1.8 mg/g obtained by the model. This indicated the suitability and accuracy of the proposed model.

3.4 Effect of interactive variables

The response surface plots of the second-order polynomial equation with one variable were kept constant, and those of other two which varied within the determined experimental ranges, are shown in Fig. 7. The response surface plots show the effects of MCP dosage, particle size, and pH on the adsorption of chromium onto MCP. This indicates that chromium adsorption increased with decreasing initial pH. This could be explained by the zero point of charge of the adsorbent (pHZ = 6.5). The MCP surface has a positive charge when the solution pH is less than pHZ, thus chromium adsorption increases. In a solution with pH > pHZ, MCP surface becomes negatively charged and decreases chromium adsorption. Contour response surface plots showing the effect of adsorbent dosage and particle size of MCP on chromium adsorption by MCP. The chromium adsorption of MCP increased with an increase in adsorbent dosage

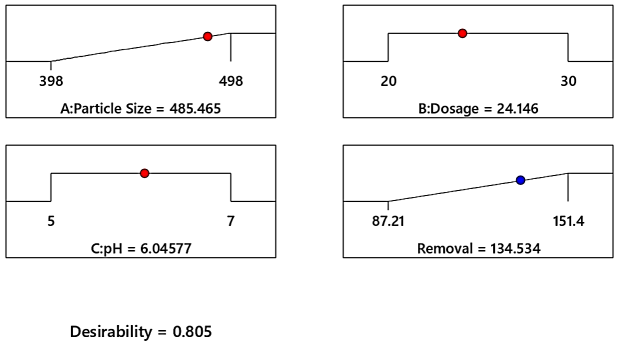

Fig. 6 Desirability graph for removal of chromium from aqueous solution

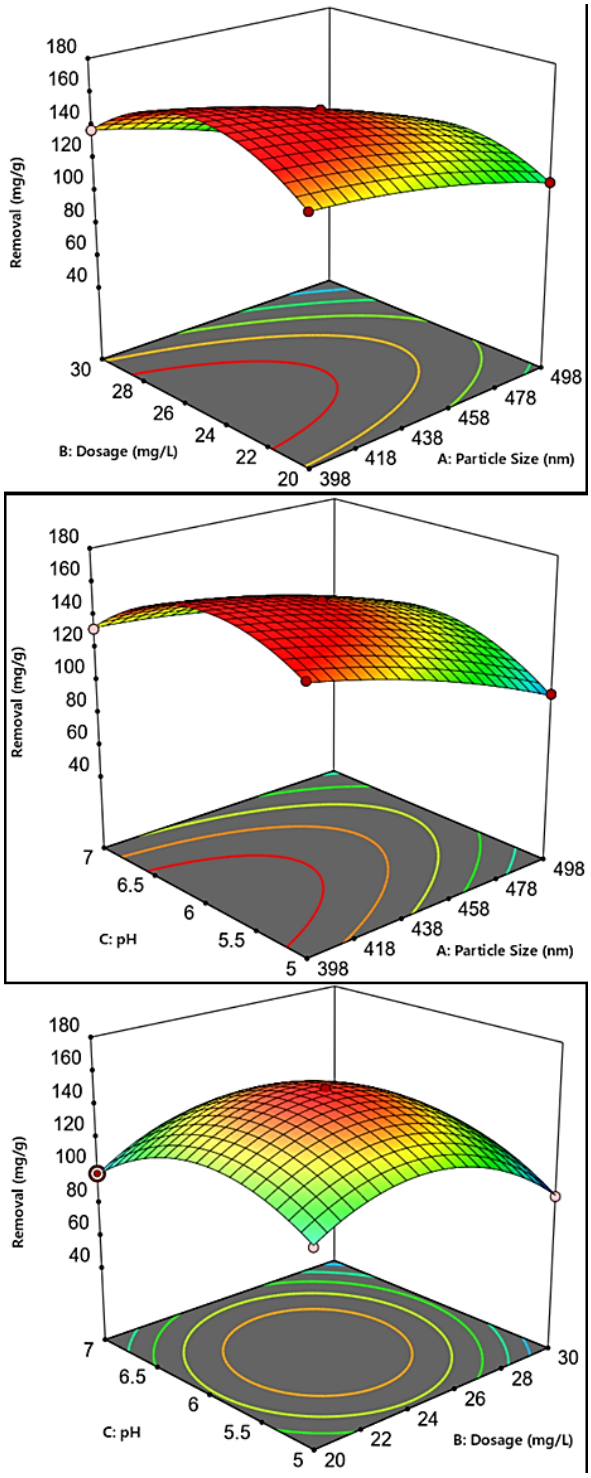

Fig. 7 Response surface plots for the adsorption of chromium on MCP

from 20–25 mg/L but a further increase in adsorbate concentration showed a slight decrease. Chromium adsorption increases along with an increase in pH from 5 to 6 for MCP. However, a further increase in the adsorbate concentration shows a slight decrease. The reason for this observation may be that the surface becomes neutral at pH 7 which reduces the adsorption of chromium onto the adsorbent. A more acidic pH is required to produce a positive charge on the surface of cellulose, which attracts metal ions from the aqueous solutions. The adsorption properties of MCP were evaluated using isotherm and kinetic models to elucidate the mechanism of chromium uptake. Recent comparative studies have indicated that the Langmuir model provides the best description of monolayer adsorption processes involving modified biomass adsorbents [40–42]. Kinetic analyses generally revealed that the pseudo-second-order model accurately represents chemisorption processes, a trend supported by our results. Compared to adsorbents derived from activated carbon [43], MCP exhibits enhanced performance and broader applicability for the chromium removal.

3.5 Adsorption isotherm and kinetics

Fig. 8 illustrates the isotherm models and kinetics fitted to the experimental data obtained at 303 K. The determined

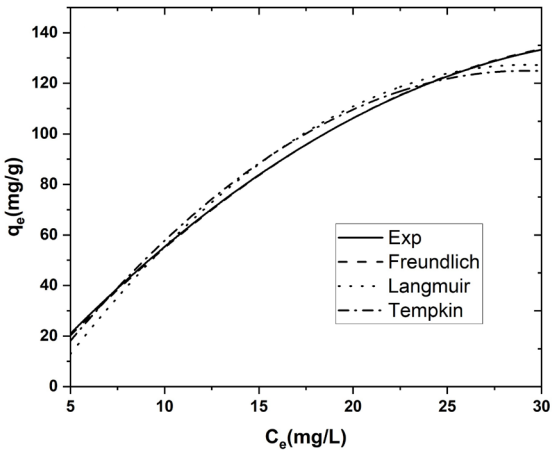

(a)

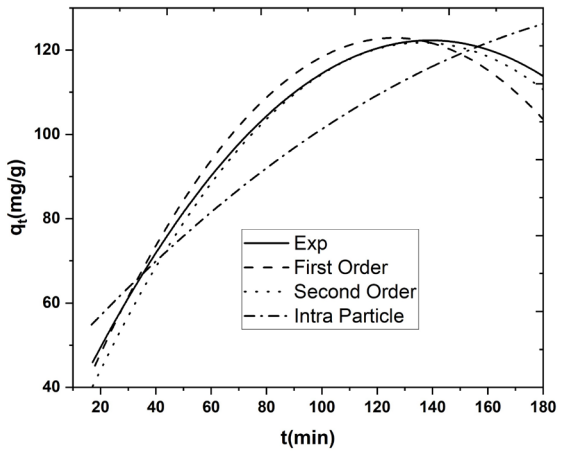

(b)

Fig. 8 (a) Adsorption isotherms of chromium onto MCP at T = 303 K, (b) adsorption kinetics of chromium onto MCP at 25 mg/L

error function values and isotherm parameters are presented in Table 4. According to Table 4, the Langmuir and Temkin isotherms showed a better fit to the adsorption data than the Freundlich isotherm for the adsorption of chromium, based on the highest R^2 value and the lowest SSE, RMSE, and R^2 values. At T = 293 K, the AIC_C values were calculated for the Langmuir (−6.827) and Temkin (−1.51) isotherms. A smaller AIC_C value suggested that the Langmuir isotherm was a better fit. The evidence ratio of 14.28 means that it is 14.28 times more likely to be the correct model than the Temkin isotherm. Therefore, the experimental results suggest that a monolayer of chromium ions is adsorbed on homogeneous adsorption sites on the surface of the MCP. The Langmuir maximum adsorption monolayer capacities were found to be 132.52 ± 2.1 mg/g at 303 K respectively. The MCP examined in this study demonstrated the highest adsorption capacity compared to most other adsorbents in terms of chromium capacity [44]. The adsorption kinetics were studied at a temperature of 303 K; particle size of 485 nm; adsorbent dose 25 mg/L and pH 6.1–6.2 Fig. 8(b) shows the kinetic models fitted to the experimental data. Similarly, all the values of the different kinetic parameters, as shown in Table 5, were obtained from various graphical presentations of the kinetic equations. The highest R^2 value and the lowest SSE, RMSE, R^2 and AIC_C values were obtained for the pseudo-second-order kinetic model. In addition, the values of $q_{e,exp}$ (132.52 ± 2.1 mg/g) and $q_{e,cal}$ (133.14 ± 3.2 mg/g) were very close to each other. Therefore, the adsorption is expected to follow pseudo-second-order kinetics.

Table 4 Chromium adsorption isotherm parameters by MCP polymer at 303 K

Langmuir		Freundlich		Temkin	
Q_L	132.52	K_F	38	K_T	121.57
b	0.051	1/n	1.738	b_T	0.165
R^2	0.9989	R^2	0.9970	R^2	0.9990
SSE	5.841	SSE	28.42	SSE	7.98
RMSE	0.5861	RMSE	1.293	RMSE	0.6853
χ^2	0.049	χ^2	0.248	χ^2	0.072
AIC_C	−6.827	AIC_C	20.07	AIC_C	−1.51

Units of parameters — Q_L: mg/g; K_F: (mg g^{-1})(L mg^{-1}); K_T: L/g; b(Langmuir): L/mg; b_T(Tempkin): J/mol

Table 5 Chromium adsorption kinetics parameters by MCP dosage of 25 mg/L at 303 K

Pseudo-first		Pseudo-second		Intra particle	
q_e	118.79	q_e	133.14	q_e	103.45
k_1	0.087	k_2	0.0053	k_i	0.581
R^2	0.9981	R^2	0.9992	R^2	0.9986
SSE	18.76	SSE	9.514	SSE	14.03
RMSE	1.050	RMSE	0.765	RMSE	0.908
χ^2	0.165	χ^2	0.098	χ^2	0.124
AIC_C	13.01	AIC_C	2.32	AIC_C	8.07

Units of parameters — k_1, k_2, k_i: (g/(mg·min)); q_e: (mg/g)

The practical effectiveness of an adsorbent depends on its regeneration ability and the use of an efficient, cost-effective, and environment-friendly desorbing agent. Our earlier research on polyadsorbents modified cellulose-triazole (MC-Tz) showed that acidic eluents like 0.1 M HCl, H_2SO_4, and CH_3COOH enabled effective desorption and reusability [45]. Using similar eluents for MCP (Fig. 9), we found that both mineral and organic acids at low concentrations successfully regenerated the material with a slight decrease in the adsorption capacity after multiple cycles. To assess the stability of MCP, we performed an FTIR analysis of the regenerated material. The characteristic functional groups of cellulose remained visible, including the C–O and C–O–C stretching region (1000–1200 cm^{-1}), although several peaks showed systematic shifts: O–H stretching shifted from 3341 to 3617 cm^{-1}, C–H stretching from 2891 to 2860 cm^{-1}, C=N stretching from 1666 to 1713 cm^{-1}, and CH_2 deformation from 1448 to 1576 cm^{-1}.

These changes were attributed to variations in hydrogen bonding and local polarity, rather than structural degradation, from the adsorption–desorption cycles. The persistence of the major functional groups indicates that MCP maintains its structural integrity after regeneration, demonstrating its durability and suitability for wastewater treatment.

The adsorption capacity of MCP for Cr(III) was 132.52 ± 2.1 mg/g at pH 6.04 ± 0.05, a dosage of 24.14 ± 0.5 mg/L, and a particle size of 485 nm, outperforming the most natural and engineered adsorbents reported in the literature (Table 6). Acid-treated

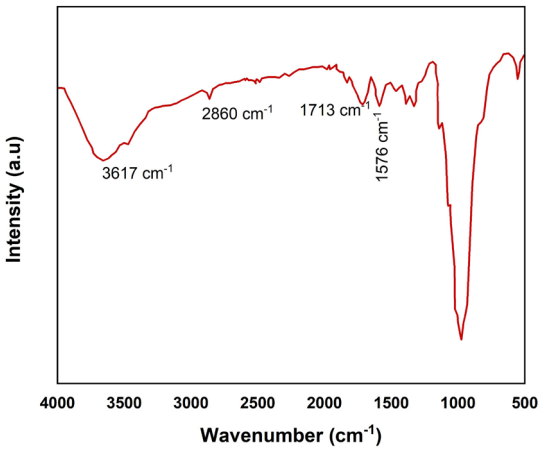

Fig. 9 FTIR spectrum of regenerated MCP after multiple adsorption cycles

Table 6 Comparative adsorption studies of the MCP with existing literatures

Adsorbent	Adsorbate	Adsorption capacity (mg/g)	Experimental conditions (pH, adsorbent dose)	Reference
Acid-treated clinoptilolite	Fluoride	1.19	pH 3; dose 20 g/L; LT*	[40]
Fe_3O_4@GO nanocomposite	Cefixime (CEX)	31	pH 3; dose 10–50 mg/L; LT	[41]
Magnetic Multi-walled Carbon Nanotube	Ciprofloxacin (CIP)	96.42	pH 3–9; dose 0.1–1 g/L; 303 K	[42]
Oak fruit derived activated carbon	Methylene blue	80–95	pH 6–7; dose 25 mg/L; 303 K	[43]
Saccharomyces cerevisiae bioadsorbent	Amoxicillin	6.27	pH 2–8; dose 0.75 g/L; 303 K	[46]
AC-ZnO nanocomposite	Diazinon	44	pH 5; dose 0.83 g/L; LT	[47]
Polyaniline-coated cellulose	Cr(VI)	35.97	pH 7; dose 4 g/L; 303 K	[48]
Modified Cellulose	Cr(III)	83.33	pH 5; dose 0.1 g/L; 303 K	[49]
Fe_3O_4/activated carbon (Banana peel)	Basic Blue 41 dye	148.5	pH 9; dose 0.5 g/L; LT	[50]
Modified Cellulose Polymer MCP (this work)	Cr(III)	132.52 ± 2.1	pH 6.04; dose 24.14 mg/L; particle size 485 nm; 30 K	This study

* LT = Laboratory temperature

clinoptilolite adsorption achieved 1.19 mg/g for fluoride [40]. MCP exceeded advanced nanomaterials such as Fe_3O_4@GO nanocomposites, which absorbed 31 mg/g of cefixime [41], and magnetic multi-walled carbon nanotubes, with 96.42 mg/g of ciprofloxacin [42]. Oak fruit–derived activated carbon showed a moderate capacity of 80-95 mg/g for methylene blue [43]. Saccharomyces cerevisiae biosorbent absorbed 6.27 mg/g of amoxicillin [46] while AC–ZnO nanocomposite achieved 44 mg/g for diazinon [47]. In chromium studies, MCP outperformed polyaniline-coated cellulose, with 35.97 mg/g for Cr(VI) at pH 7 and 4 g/L, and unmodified cellulose, with 83.33 mg/g for Cr(III) at pH 5 and 0.1 g/L [48, 49]. Only Fe_3O_4/activated carbon from banana peel slightly outperformed MCP with 148.5 mg/g for Basic Blue 41 dye at pH 9 [50]. These comparisons show that MCP outperforms most natural, cellulose-based, and engineered adsorbents for heavy metals while rivaling advanced composite systems and maintaining eco-friendly, renewable, and easy synthesis benefits.

4 Conclusion

Environmental issues have prompted extensive research into industrial adsorbents. In response, a novel, cost-effective sorbent has been developed using cellulose, a material that is abundant, biodegradable, and structurally stable. The incorporation of polymeric chelating moieties containing diverse O, N, and S donor atoms into the cellulose backbone results in high extraction efficiency for metals from aqueous solutions. These heteroatoms facilitate the attraction of metal ions to aqueous solutions and enable their complexation. In this study, the statistical methodology, Box–Behnken response surface design, was demonstrated to be effective and reliable for determining the optimal conditions for the adsorption of chromium onto MCP. The results indicated that the adsorption conditions significantly affected the removal of chromium. Response surface plots were used to estimate the interactive effect of three independent variables (particle size in nm, pH, and adsorbent dose) on the response (chromium adsorption). A second-order mathematical model was developed through regression analysis of the experimental data obtained from 17 batch runs. Applying the desirability function method, the optimization of the adsorbent dose (24.14 ± 0.5 mg/L), particle size (485.49 ± 2 nm), and pH (6.04 ± 0.05) yielded a maximum chromium adsorption of 134.53 ± 1.8 mg/g with a desirability of 0.805. Various kinetic models were examined, and the pseudo-second-order model was found to be applicable in this study. Langmuir, Freundlich, and Temkin isotherm models were employed to describe the adsorption equilibrium of chromium. These data are in good agreement with the Langmuir isotherm. The findings of this study indicate that MCP possesses a substantial adsorption capability, and further optimization enhances its commercial viability.

Acknowledgement

The authors express their gratitude to the KPR Institute of Engineering and Technology, Coimbatore, for generously providing the necessary research facilities and characterization support for this study.

References

[1] Kolopajlo, L. "Chapter 5 A review of sustainable leather tanning", In: Benvenuto, M. A. (ed.) Green Chemical Processes: Developments in Science, Math, Engineering and Technology, De Gruyter, 2024, pp. 67–150. ISBN 9783110799088 https://doi.org/10.1515/9783110799088-005

[2] Kumar, M., Saini, H. S. "Novel Approaches for Sustainable Management of Chromium Contaminated Wastewater in Wastewater Treatment and Sludge Management Systems - The Gutter-to-Good Approaches", Intechopen, 2024. ISBN 978-0-85466-742-0 https://doi.org/10.5772/intechopen.1003944

[3] Georgaki, M.-N., Charalambous, M., Kazakis, N., Talias, M. A., Georgakis, C., Papamitsou, T., Mytiglaki, C. "Chromium in water and carcinogenic human health risk", Environments, 10(2), 33, 2023. https://doi.org/10.3390/environments10020033

[4] Ayach, J., El Malti, W., Duma, L., Lalevée, J., Al Ajami, M., Hamad, H., Hijazi, A. "Comparing conventional and advanced approaches for heavy metal removal in wastewater treatment: an in-depth review emphasizing filter-based strategies", Polymers, 16(14), 1959, 2024. https://doi.org/10.3390/polym16141959

[5] Venkatachalam, D., Kaliappa, S. "Superabsorbent polymers: a state-of-art review on their classification, synthesis, physico-chemical properties, and applications", Reviews in Chemical Engineering, 39(1), pp. 127–171, 2023. https://doi.org/10.1515/revce-2020-0102

[6] Zhao, C., Liu, G., Tan, Q., Gao, M., Chen, G., …, Xu, D. "Polysaccharide-based biopolymer hydrogels for heavy metal detection and adsorption", Journal of Advanced Research, 44, pp. 53–70, 2023. https://doi.org/10.1016/j.jare.2022.04.005

[7] Etale, A., Onyianta, A. J., Turner, S. R., Eichhorn, S. J. "Cellulose: A Review of Water Interactions, Applications in Composites, and Water Treatment", Chemical Reviews, 123(5), pp. 2016–2048, 2023. https://doi.org/10.1021/acs.chemrev.2c00477

[8] Sinha, S., Nigam, S., Solanki, S., Batra, L., Chug, P., Singh, R. "Prospects on arsenic remediation using organic cellulose-based adsorbents", Industrial Crops and Products, 201, 116928, 2023. https://doi.org/10.1016/j.indcrop.2023.116928

[9] Arredondo, R., Yuan, Z., Sosa, D., Johnson, A., Beims, R. F., Li, H., Wei, Q., Xu, C. C. "Performance of a novel, eco-friendly, cellulose-based superabsorbent polymer (Cellulo-SAP): Absorbency, stability, reusability, and biodegradability", Canadian Journal of Chemical Engineering, 101(4), pp.1762–1771, 2023. https://doi.org/10.1002/cjce.24601

[10] Saravanan, R., Ravikumar, L. "The use of new chemically modified cellulose for heavy metal ion adsorption and antimicrobial activities", Journal of water resource and protection, 7(6), pp. 530–545, 2015. https://doi.org/10.4236/jwarp.2015.76042

[11] Saravanan, R., Ravikumar, L. "Renewable Modified Cellulose Bearing Chelating Schiff Base for Adsorptive Removal of Heavy Metal Ions and Antibacterial Action", Water Environment Research, 89(7), pp. 629–640, 2017. https://doi.org/10.2175/106143016X14733681696329

[12] Rajayyan, S., Lingam, R. "Adsorption equilibrium and kinetic studies on effective removal of heavy metals onto modified cellulose bearing Schiff base with pyridine chelating groups from aqueous solution", International Journal of Materials and Product Technology, 55(1–3), pp. 188–209, 2017. https://doi.org/10.1504/IJMPT.2017.084967

[13] Saravanan, R., Ravikumar, L. "Cellulose bearing Schiff base and carboxylic acid chelating groups: a low cost and green adsorbent for heavy metal ion removal from aqueous solution", Water Science and Technology, 74(8), pp. 1780–1792, 2016. https://doi.org/10.2166/wst.2016.296

[14] Saravanan, R., Mahalakshmi, R., Karthikeyan, M. S., Ravikumar, L. "Chelating modified cellulose bearing pendant heterocyclic moiety for effective removal of heavy metals", Water Science and Technology, 80(8), pp. 1549–1561, 2019. https://doi.org/10.2166/wst.2019.404

[15] Yusuff, A. S., Ishola, N. B., Gbadamosi, A. O., Epelle, E. I. "Modeling and optimization of hexavalent chromium adsorption by activated Eucalyptus biochar using response surface methodology and adaptive neuro-fuzzy inference system", Environments, 10(3), 55, 2023. https://doi.org/10.3390/environments10030055

[16] Nadeem Zafar, M., Dargahi, A., Pirdadeh, F. "Synthesis of magnesium oxide nanoparticles and its application for photocatalytic removal of furfural from aqueous media: Optimization using response surface methodology", Arabian Journal of Chemistry, 16(8), 104998, 2023. https://doi.org/10.1016/j.arabjc.2023.104998

[17] Hasani, K., Peyghami, A., Moharrami, A., Vosoughi, M., Dargahi, A. "The efficacy of sono-electro-Fenton process for removal of Cefixime antibiotic from aqueous solutions by response surface methodology (RSM) and evaluation of toxicity of effluent by microorganisms", Arabian Journal of Chemistry, 13(7), pp. 6122–6139, 2020. https://doi.org/10.1016/j.arabjc.2020.05.012

[18] Heidari, M., Vosoughi, M., Sadeghi, H., Dargahi, A., Mokhtari, S. A. "Degradation of diazinon from aqueous solutions by electro-Fenton process: effect of operating parameters, intermediate identification, degradation pathway, and optimization using response surface methodology (RSM)", Separation Science and Technology, 56(13), pp. 2287–2299, 2021. https://doi.org/10.1080/01496395.2020.1821060

[19] Afshin, S., Rashtbari, Y., Vosough, M., Dargahi, A., Fazlzadeh, M., Behzad, A., Yousefi, M. "Application of Box–Behnken design for optimizing parameters of hexavalent chromium removal from aqueous solutions using Fe_3O_4 loaded on activated carbon prepared from alga: kinetics and equilibrium study", Journal of Water Process Engineering, 42, 102113, 2021. https://doi.org/10.1016/j.jwpe.2021.102113

[20] Samarghandi, M. R., Dargahi, A., Rahmani, A., Shabanloo, A., Ansari, A., Nematollahi, D. "Application of a fluidized three-dimensional electrochemical reactor with Ti/SnO_2–Sb/β-PbO_2 anode and granular activated carbon particles for degradation and mineralization of 2, 4-dichlorophenol: process optimization and degradation pathway", Chemosphere, 279, 130640, 2021. https://doi.org/10.1016/j.chemosphere.2021.130640

[21] Dargahi, A., Barzoki, H. R., Vosoughi, M., Mokhtari, S. A. "Enhanced electrocatalytic degradation of 2, 4-Dinitrophenol (2, 4-DNP) in three-dimensional sono-electrochemical (3D/SEC) process equipped with Fe/SBA-15 nanocomposite particle electrodes: degradation pathway and application for real wastewater", Arabian Journal of Chemistry, 15(5), 103801, 2022. https://doi.org/10.1016/j.arabjc.2022.103801

[22] Dargahi, A., Vosoughi, M., Mokhtari, S. A., Vaziri, Y., Alighadri, M. "Electrochemical degradation of 2, 4-Dinitrotoluene (DNT) from aqueous solutions using three-dimensional electrocatalytic reactor (3DER): degradation pathway, evaluation of toxicity and optimization using RSM-CCD", Arabian Journal of Chemistry, 15(3), 103648, 2022. https://doi.org/10.1016/j.arabjc.2021.103648

[23] Pourali, P., Fazlzadeh, M., Aaligadri, M., Dargahi, A., Poureshgh, Y., Kakavandi, B. "Enhanced three-dimensional electrochemical process using magnetic recoverable of Fe_3O_4@GAC towards furfural degradation and mineralization", Arabian Journal of Chemistry, 15(8), 103980, 2022. https://doi.org/10.1016/j.arabjc.2022.103980

[24] Furniss, B. S., Hannaford, A. J., Smith, P. W. G., Tatchell, A. R. "Vogel's Textbook of Practical Organic Chemistry, 1989", Singapore, Longman, 1989. ISBN 0582462363

[25] Brault, L., Marlin, N., Mortha, G., Boucher, J., Lachenal, D. "About the Assessment of the Degree of Oxidation of Cellulose During Periodate Reaction: Comparison of Different Characterization Techniques and Their Discrepancies", Carbohydrate Research, 552, 109438, 2025. https://doi.org/10.1016/j.carres.2025.109438

[26] El Mahdaoui, A., Radi, S., Elidrissi, A., Faustino, M. A. F., Neves, M. G. P., Moura, N. M. "Progress in the modification of cellulose-based adsorbents for the removal of toxic heavy metal ions", Journal of Environmental Chemical Engineering, 12(5), 113870, 2024. https://doi.org/10.1016/j.jece.2024.113870

[27] Buenaño, L., Ali, E., Jafer, A., Zaki, S. H., Hammady, F. J., Khayoun Alsaadi, S. B., Karim, M. M., Ramadan, M. F., Omran, A. A., Alawadi, A. "Optimization by Box–Behnken design for environmental contaminants removal using magnetic nanocomposite", Scientific Reports, 14, 6950, 2024. https://doi.org/10.1038/s41598-024-57616-8

[28] Chemingui, H., Rezma, S., Lafi, R., Alhalili, Z., Missaoui, T., Harbi, I., Smiri, M., Hafiane, A. "Investigation of methylene blue adsorption from aqueous solution onto ZnO nanoparticles: equilibrium and Box-Behnken optimisation design", International Journal of Environmental Analytical Chemistry, 103(12), pp. 2716–2741, 2023. https://doi.org/10.1080/03067319.2021.1897121

[29] Arslane, M., Slamani, M., Elhadi, A., Amroune, S. "Multi-response optimization of drilling parameters in hybrid natural fiber composites using Taguchi and desirability function analysis (DFA)", The International Journal of Advanced Manufacturing Technology, 135(11), pp. 5631–5645, 2024. https://doi.org/10.1007/s00170-024-14855-3

[30] Ćujić, S., Jankov, M., Ristivojević, P., Andrić, F. "Multiobjective optimization of effect-directed planar chromatography as a promising tool for fast selection of polypotent natural products", Journal of Chromatography A, 1732(13), 465252, 2024. https://doi.org/10.1016/j.chroma.2024.465252

[31] Kushwaha, J., Singh, R. "Cellulose hydrogel and its derivatives: A review of application in heavy metal adsorption", Inorganic Chemistry Communications, 152, 110721, 2023. https://doi.org/10.1016/j.inoche.2023.110721

[32] Kausar, A. "Polymeric nanocomposite via electrospinning: Assessment of morphology, physical properties and applications", Journal of Plastic Film & Sheeting, 37(1), pp. 70–92, 2021. https://doi.org/10.1177/8756087920937344

[33] Naderahmadian, A., Eftekhari-Sis, B., Jafari, H., Zirak, M., Padervand, M., Mahmoudi, G., Samadi, M. "Cellulose nanofibers decorated with SiO_2 nanoparticles: Green adsorbents for removal of cationic and anionic dyes; kinetics, isotherms, and thermodynamic studies", International Journal of Biological Macromolecules, 247, 125753, 2023. https://doi.org/10.1016/j.ijbiomac.2023.125753

[34] Ho, Y.-S., McKay, G. "Pseudo-second order model for sorption processes", Process Biochemistry, 34, pp.451–465, 1999. https://doi.org/10.1016/S0032-9592(98)00112-5

[35] Mao, J., Lei, X., Fu, X., Chen, Z., Zhu, H., Xue, F., Yu, Z., Wang, L., Xia, N., He, H. "Structural design of cellulose-hyperbranched double-network for enhanced intramolecular diffusion kinetics of heavy metal ion capture processes", Chemical Engineering Journal, 498, 155642, 2024. https://doi.org/10.1016/j.cej.2024.155642

[36] Laskar, A. A., Ahmed, M., Vo, D.-V. N., Abdullah, A., Shahadat, M., Mahmoud, M. H., Khan, W., Yusuf, M. "Mathematical modeling and regression analysis using MATLAB for optimization of microwave drying efficiency of banana", Thermal Science and Engineering Progress, 46, 102157, 2023. https://doi.org/10.1016/j.tsep.2023.102157

[37] Wu, R., Kashi, E., Jawad, A. H., Musa, S. A., ALOthman, Z. A., Wilson, L. D. "Polymeric Matrix of Modified Chitosan with Algae and Coal Fly Ash for a Toxic Cationic Dye Removal: Multivariable Optimization by Box-Behnken Design", Journal of Inorganic and Organometallic Polymers and Materials, 35, pp. 2300–2314, 2024. https://doi.org/10.1007/s10904-024-03241-x

[38] Abdulhameed, A. S., Al Omari, R. H., Abualhaija, M., Algburi, S. "Chitosan polymer/ functionalised rambutan peel using carboxylic acid: process optimisation using Box-Behnken Design for brilliant green dye removal", International Journal of Environmental Analytical Chemistry, 2024. https://doi.org/10.1080/03067319.2024.2392638

[39] Ali, H. R., Mostafa, H. Y., Husien, S., El-hoshoudy, A. N. "Adsorption of BTX from produced water by using ultrasound-assisted combined multi-template imprinted polymer (MIPs); factorial design, isothermal kinetics, and Monte Carlo simulation studies", Journal of Molecular Liquids, 370, 121079, 2023. https://doi.org/10.1016/j.molliq.2022.121079

[40] Mahmoudi, M. M., Nasseri, S., Mahvi, A. H., Dargahi, A., Khubestani, M. S., Salari, M. "Fluoride removal from aqueous solution by acid-treated clinoptilolite: isotherm and kinetic study", Desalination and Water Treatment, 146, pp. 333–340, 2019. https://doi.org/10.5004/dwt.2019.23625

[41] Mahdavian, F., Dargahi, A., Vosoughi, M., Mokhtari, A., Sadeghi, H., Rashtbari, Y. "Enhanced removal of cefixime from aqueous solutions using Fe_3O_4@GO nanocomposite with ultrasonic: isotherm and kinetics study", Desalination and Water Treatment, 280, pp. 224–239, 2022. https://doi.org/10.5004/dwt.2022.29111

[42] Shokoohi, R., Dargahi, A., Azami Gilan, R., Zolghadr Nasab, H., Zeynalzadeh, D., Molla Mahmoudi, M. "Magnetic Multi-walled Carbon Nanotube as Effective Adsorbent for Ciprofloxacin (CIP) Removal from Aqueous Solutions: Isotherm and Kinetics Studies", International Journal of Chemical Reactor Engineering, 18(2), 20190130, 2020. https://doi.org/10.1515/ijcre-2019-0130

[43] Seidmohammadi, A., Asgari, G., Dargahi, A., Leili, M., Vaziri, Y., Hayati, B., Shekarchi, A. A., Mobarakian, A., Bagheri, A., Nazari Khanghah, S. B. "A comparative study for the removal of methylene blue dye from aqueous solution by novel activated carbon based adsorbents", Progress in Color, Colorants and Coatings, 12, pp. 133–144, 2019. https://doi.org/10.30509/pccc.2019.81551

[44] Hashem, M. A., Mim, M. W., Noshin, N., Maoya, M. "Chromium adsorption capacity from tannery wastewater on thermally activated adsorbent derived from kitchen waste biomass", Cleaner Water, 1, 100001, 2024. https://doi.org/10.1016/j.clwat.2023.100001

[45] Mahalakshmi, R., Saravanan, R., Selvakumar, P., Karthikeyan, M. S., Ravikumar, L. "Polymeric Substitution of Triazole Moieties in Cellulosic Schiff Base for Heavy Metal Complexation Studies", Journal of Polymer Environment, 30, pp. 360–372, 2022. https://doi.org/10.1007/s10924-021-02201-7

[46] Samarghandi, M. R., Asgari, G., Shokoohi, R., Dargahi, A., Arabkouhsar, A. "Removing amoxicillin antibiotic from aqueous solutions by Saccharomyces cerevisiae bioadsorbent: kinetic, thermodynamic and isotherm studies", Desalination and Water Treatment, 152, pp. 306–315, 2019. https://doi.org/10.5004/dwt.2019.23941

[47] Pourali, P., Rashtbari, Y., Behzad, A., Ahmadfazeli, A., Poureshgh, Y., Dargahi, A. "Loading of zinc oxide nanoparticles from green synthesis on the low cost and eco-friendly activated carbon and its application for diazinon removal: isotherm, kinetics and retrieval study", Applied Water Science, 13(4), 101, 2023. https://doi.org/10.1007/s13201-023-01871-z

[48] Dewa, L., Tichapondwa, S.M., Mhike, W. "Adsorption of hexavalent chromium from wastewater using polyaniline-coated microcrystalline cellulose nanocomposites", RSC Advances, 14(10), pp. 6603–6616, 2024. https://doi.org/10.1039/D3RA08027G

[49] Daniel, A. B., Zahir, E., Hussain, I., Naz, S., Asghar, M. A. "Citric acid modified cellulose: a cost-effective adsorbent for the immobilization of Cr (III) ions from the aqueous phase", Energy Sources, Part A: Recovery, Utilization, and Environmental Effects, 46(1), pp. 9024–9036, 2024. https://doi.org/10.1080/15567036.2020.1773963.

[50] Mohammadifard, A., Allouss, D., Vosoughi, M., Dargahi, A., Moharrami, A. "Synthesis of magnetic Fe_3O_4/activated carbon prepared from banana peel (BPAC@Fe_3O_4) and salvia seed (SSAC@Fe_3O_4) and applications in the adsorption of Basic Blue 41 textile dye from aqueous solutions", Applied Water Science, 12(5), 88, 2022. https://doi.org/10.1007/s13201-022-01622-6